Geophysical Journal International

Geophys. J. Int. (2014) **197,** 591–607
Advance Access publication 2014 February 11

doi: 10.1093/gji/ggu012

Analysing seismic convex topographies by a half-plane time-domain BEM

M. Panji,[1] M. Kamalian,[2] J. Asgari Marnani[3] and M. K. Jafari[2]

[1]*Department of Civil Engineering, Zanjan Branch, Islamic Azad University, Zanjan, Iran. E-mail: m.panji@srbiau.ac.ir*
[2]*Geotechnical Engineering Research Center, International Institute of Earthquake Engineering and Seismology, Tehran, Iran*
[3]*Department of Civil Engineering, Technical and Engineering Faculty, Central Tehran Branch, Islamic Azad University, Tehran, Iran*

Accepted 2014 January 13. Received 2014 January 2; in original form 2013 June 20

SUMMARY

This paper extends a method, which has been previously called half-plane time-domain boundary element method (BEM) and successfully applied to 2-D concave topographies, for analysing convex irregular sites subjected to vertically as well as obliquely propagating incident *SH* waves. While using this method, only interface and surface of the hill needed to be discretized. During the use of the proposed substructuring process and dividing the problem into two domains of a half-space and a surface topography totally above the half-space, the method was employed for each of them. After satisfying continuity and boundary conditions, the problem was finally solved as an original coupled domain. To validate the presented method, three different examples were examined and the results were compared with those of the published works. A semi-circular cylindrical hill, a Gaussian-shaped ridge and a semi-circular hill joined by an inside concentric full/semi-circular cavity were investigated due to antiplane waves as Ricker wavelets type. The results showed that not only capability and efficiency of the method were very good but also much shorter run time than that of full-plane BEM formulation was obtained. The proposed method can be practically used to analyse site response in substituting traditional time-domain BEM as well.

Key words: Site effects; Computational seismology; Wave scattering and diffraction; Wave propagation.

1 INTRODUCTION

Recent earthquakes as well as their subsequent events have shown that amplitude of ground motion not only is related to earthquake intensity but also depends on the site geometry. Technically speaking, there are generally three different methods for the analysis of topographic effects which include analytical, semi-analytical and numerical ones (Sanchez-Sesma *et al.* 2002). Although analytical and semi-analytical methods have better accuracy than numerical approaches, various types of arbitrarily shaped topographic features cannot be applied for modelling in real world. It results in the development of numerical methods which have good flexibility. Among the numerical methods, which can be commonly divided to volumetric, boundary and mixed, special attention has been given to boundary element method (BEM) during recent two decades. Due to the fact that this method only discretizes boundaries of the media and automatically satisfies the Sommerfeld's radiation conditions of waves at infinity, its application for analysing the infinite and semi-infinite continuous media is really suitable (Beskos 1997).

Although boundary element formulation for a linear elastic medium has been developed in both time and frequency domains, non-linear analysis of different problems in combination with other numerical methods, analysis of problems with time-dependent geometry and also obtaining real values are only possible by the assistance of step-by-step process in the former. Perhaps, Friedman & Shaw (1962) could be known as pioneer researchers in the use of time-domain BEM for antiplane wave scattering problems. Cole *et al.* (1978) were able to present the first form of full-plane time-domain BEM approach together with its scalar time-convoluted kernels. But, due to low precision of their displacement kernels, they have not been developed. Mansur & Brebbia (1982a,b) introduced a general full-plane time-domain BEM for antiplane elastodynamic problems including displacement and traction time-convoluted kernels. Because of their consideration of the Heaviside function in the extraction of formulations, their results have been reported in terms of different wave front positions. To follow Mansur's studies, Demirel & Wang (1987), Dominguez (1993), Yu *et al.* (2000) and Soares & Mansur (2009) have manages to improve the full-plane time-domain BEM and demonstrate a better view for them. In this regard, the full-plane time-domain BEM approach presented by Israil & Banerjee (1990a) had the most stylish results until that time. These researchers, unlike the previous authors and regardless of the Heaviside function, were able to extract antiplane kernels in a condensed closed form. Later, Kamalian *et al.* (2003) modified their in-plane

kernels (Israil & Banerjee 1990b) and applied them in time-domain BEM code for analysing different geotechnical earthquake problems (Kamalian *et al.* 2006, 2007, 2008a,b). Recently, a half-plane time-domain BEM approach as well as its condensed closed-form half-plane time-convoluted kernels were presented by Panji *et al.* (2013a) and used for investigating seismic behaviour of concave surface topographies joined by embedded cavities (Panji *et al.* 2013b,c).

Despite the fact that solving the hill problems has been considerable for he researchers due to propagating incident *SH* waves either with the assistance of analytical methods (Sabina & Willis 1975; Yuan & Men 1992; Yuan & Liao 1996; Lee *et al.* 2006; Tsaur & Chang 2009; Jaramillo *et al.* 2013, for single topography effects and Lee *et al.* 2004; Liang *et al.* 2004; Liu *et al.* 2010, for multiple topography effects) or by semi-analytical techniques (Bouchon 1973; Bard 1982; Geli *et al.* 1988; Zhou & Chen 2006, 2008; Chen *et al.* 2012), using BEM approaches has been rarely observed in the literature. Sills (1978) developed an indirect frequency-domain BEM and applied it for analysing the Gaussian-shaped hills. In the use of a boundary method, Sanchez-Sesma *et al.* (1982) investigated the behaviour of Gaussian-shaped ridges subjected to oblique *SH* wave. Using indirect frequency-domain BEM, Sanchez-Sesma & Campillo (1991) analysed arbitrarily shaped convex topographies to *P* and *SV* waves. Mogi & Kawakami (2007) presented a sinusoidal ground model with direct frequency-domain BEM approach. Finally, Kamalian *et al.* (2008a,b) were able to analyse the elevated topographies by means of direct time-domain BEM.

Although it is possible for BEM approaches to be formulated in a full-plane or half-plane domain (Dominguez & Meise 1991), more studies have been conducted by the former one due to the simplicity of its formulations. All the above-mentioned works in the previous paragraph have been also done based on full-plane BEM approach. In the prepared models established on the full-plane BEM, not only topography surface but also a wide area of smooth ground surface from each of its sides must be discretized to approximately satisfy stress-free boundary conditions (Kamalian *et al.* 2006; Ge & Chen 2007, 2008). Besides, to avoid numerical integration difficulties, a series of virtual elements called 'enclosing elements' need to be defined to close the truncated domain (Ahmad & Banerjee 1988), which, in addition to complicating the models, also considerably increase analysis time (Kamalian *et al.* 2008a,b).

On the other hand, if the considered problem is completely solved in a half-space using half-plane BEM approaches, the dimension of elements and their runs time are subsequently reduced, due to focusing the elements only on the topography surfaces (Panji *et al.* 2013a). In addition, the stress-free boundary conditions will be also satisfied exactly on the ground surface. The half-plane BEM topography models which rough surfaces are always below the ground, such as valley-shaped topographies and underground cavities, are capable to be solved straightforwardly. Meanwhile, some studies can be found for *SH* waves scattering in the literature (Wong & Jennings 1975; Sanchez-Sesma & Esquivel 1979; Dravinski 1982; Ohtsu & Uesugi 1985; Reinoso *et al.* 1993; Ausilio *et al.* 2008 in frequency domain and Hirai 1988, Belytschko & Chang 1988 and Panji *et al.* 2013a in time domain). Nonetheless, solving convex topographies by means of half-plane BEM approach is not possible in this way and use of a proposed separation technique is thus required. To the best knowledge of the present authors, the convex topography solution completely in a half-space asking for the assistance of direct BEM approaches not only in the time but also in the frequency domain has not been conducted so far.

The authors previously proposed a half-plane time-domain BEM approach to investigate homogenous topography behaviour including concave shaped and subsurface irregularities. In this paper, the mentioned formulations were developed for convex topographies and applied in a time-domain BEM code known as DASBEM. To this end, first, using the proposed substructuring process, the convex topography (hill) was divided into two domains: the first one including a homogeneous half-space with its interface with hill as an open media model and the second one containing a surface topography totally above the half-space as a closed media model. Then, both domains were modelled based on half-plane time-domain BEM formulation. After forming influence coefficients of the required matrices for each domain, they were assembled into a global matrix, taking continuity conditions of the interface into account. Eventually the equations could be solved by applying the boundary conditions for an original coupled domain. To investigate applicability and efficiency of the proposed approach, three practical examples were solved and compared with those of published works. A semi-circular cylindrical hill, a Gaussian-shaped ridge as well as a semi-circular hill joined by an inside concentric full/semi-circular cavity were considered subjected to obliquely propagating incident *SH* waves as the Ricker wavelets type. The main objective of this paper was to demonstrate simple models for convex topographies in use of the presented half-plane time-domain BEM while considerably reducing analysis time compared with traditional full-plane models and accurately obtaining the solutions.

2 HALF-PLANE TIME-DOMAIN BEM

2.1 Governing equations

For a homogeneous linear elastic medium according to Fig. 1, 2-D scalar wave equation and boundary conditions on the surface are respectively as follows:

$$\frac{\partial^2 u(x,y,t)}{\partial x^2}+\frac{\partial^2 u(x,y,t)}{\partial y^2}+b\,(x,y,t)=\frac{1}{c^2}\frac{\partial^2 u(x,y,t)}{\partial t^2} \tag{1}$$

and

$$\mu\frac{\partial u(x,y,t)}{\partial n}\bigg|_{y=0}=0, \tag{2}$$

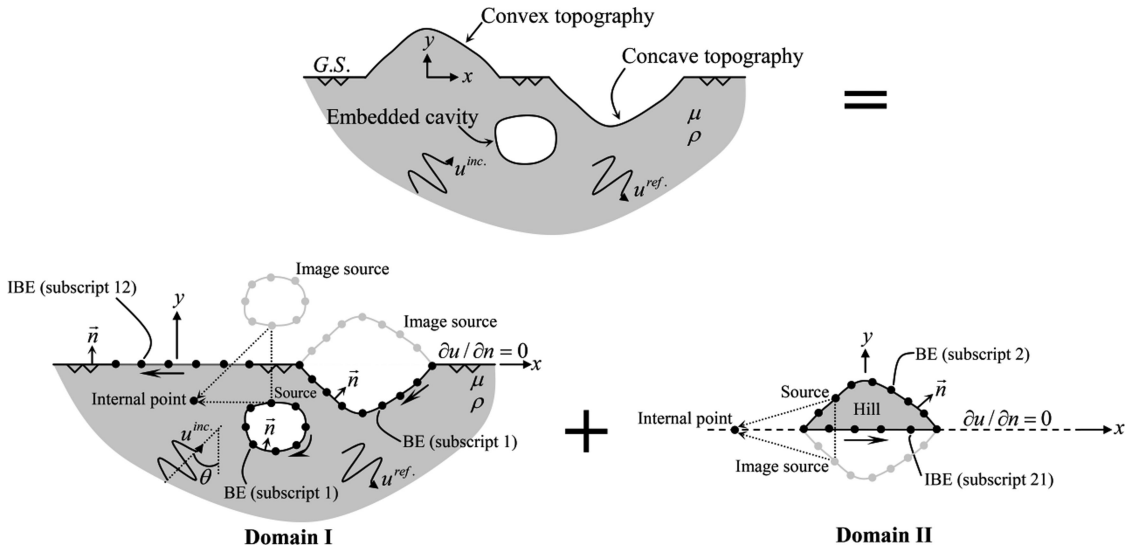

Figure 1. A definition sketch for solving the combined topography problems using half-plane time-domain BEM approach based on source image method and substructuring process. IBE and BE indicate the interface and usual boundary elements, respectively.

where $u(x, y, t)$ and $b(x, y, t)$ are antiplane displacement and body force at point (x, y) and current time t, respectively, c is shear wave velocity given by $\sqrt{\mu/\rho}$, with μ as shear modulus and ρ as mass density, and n is normal vector for the ground surface. Without considering boundary conditions (eq. 2), eq. (1) can be solved alone to obtain the full-plane fundamental solutions. Transient antiplane full-plane fundamental solutions can be found in Morse & Feshbach (1953) and Eringen & Suhubi (1975). The singular solution of governing equation by satisfying the boundary conditions as well as using image source approach results in the half-plane fundamental solutions. These solutions together with its mathematical proof can be found in Panji *et al.* (2013a).

2.2 Boundary integral equations (BIEs)

After applying the weighted residual integral to eq. (1) and ignoring contributions from initial conditions and body forces, direct time-domain BIE can be obtained as follows (Brebbia & Dominguez 1989, Dominguez 1993):

$$c(\boldsymbol{\xi})\, u(\boldsymbol{\xi}, t) = \int_{\Gamma} \left\{ \int_0^t \left[u^*(\boldsymbol{x}, t; \boldsymbol{\xi}, \tau) \cdot q(\boldsymbol{x}, \tau) - q^*(\boldsymbol{x}, t; \boldsymbol{\xi}, \tau) \cdot u(\boldsymbol{x}, \tau) \right] \mathrm{d}\tau \right\} \mathrm{d}\Gamma(\boldsymbol{x}) \tag{3}$$

u^* and q^* are half-plane time-domain displacement and traction fundamental solutions at position $\boldsymbol{x}$ and time t due to a unit antiplane impulsive force in position $\boldsymbol{\xi}$ and preceding time τ, respectively; u and q are displacements and tractions of boundary, respectively. $\Gamma(\boldsymbol{x})$ denotes the boundary of body. $c(\boldsymbol{\xi})$ is the geometry coefficient which can be obtained in terms of internal angle of the corner (Dominguez 1993). The above BIE is governed for the problems under external loads. If the problems include the incoming waves, then, to satisfy the stress-free conditions on the surface (eq. 2) with considering that total displacement can be decomposed into two parts containing the free field displacement (u^{ff}) and the scattered wave field ($u^{sc.}$), eq. (3) must be modified as (Ohtsu & Uesugi 1985; Kawase 1988; Hadley *et al.* 1989; Reinoso *et al.* 1993):

$$c(\boldsymbol{\xi})\, u(\boldsymbol{\xi}, t) = \int_{\Gamma} \left\{ \int_0^t \left[u^*(\boldsymbol{x}, t; \boldsymbol{\xi}, \tau) \cdot q(\boldsymbol{x}, \tau) - q^*(\boldsymbol{x}, t; \boldsymbol{\xi}, \tau) \cdot u(\boldsymbol{x}, \tau) \right] \mathrm{d}\tau \right\} \mathrm{d}\Gamma(\boldsymbol{x}) + u^{ff}(\boldsymbol{\xi}, t), \tag{4}$$

where u^{ff} is the free field displacement of ground surface (without surface irregularities). Once the above equation is solved for all boundary points on the topography, it is possible to determine responses for the rest of the considered points including smooth surface ($y = 0$) beyond the topography as internal fields m. Thus, by placing the geometry coefficient of $c(\boldsymbol{\xi})$ equal to 1, the above equation can be rewritten as follows:

$$u^m(\boldsymbol{\xi}, t) = \int_{\Gamma} \left\{ \int_0^t \left[u^{*m}(\boldsymbol{x}, t; \boldsymbol{\xi}, \tau) \cdot q(\boldsymbol{x}, \tau) - q^{*m}(\boldsymbol{x}, t; \boldsymbol{\xi}, \tau) \cdot u(\boldsymbol{x}, \tau) \right] \mathrm{d}\tau \right\} \mathrm{d}\Gamma(\boldsymbol{x}) + u^{ff.m}(\boldsymbol{\xi}, t), \tag{5}$$

where u^{*m} and q^{*m} are half-plane time-domain fundamental solutions for displacement and traction fields established on each of internal points, respectively, and $u^{ff.m}$ is free field displacements that must be obtained for them.

2.3 Numerical implementation

For solving BIE (eq. 4) in the time domain, it is required for the time axis and geometry boundary to be discretized. In this regard, an analytical process and a numerical scheme were considered for the former and latter.

2.3.1 *Temporal integration*

To carry out the analytical temporal integration, after discretizing the time axis by N equal increments with duration Δt ($t = N\Delta t$) in the use of linearly shaped functions, eq. (4) can be presented in the following way as a simplified form resulting from eliminating singularity terms from wave fronts:

$$c(\boldsymbol{\xi})\,u^N(\boldsymbol{\xi}) = \sum_{n=1}^{N}\int_{\Gamma}\begin{pmatrix}\left[U_1^{N-n+1}(\boldsymbol{x},\boldsymbol{\xi}) + U_2^{N-n}(\boldsymbol{x},\boldsymbol{\xi})\right]q^n(\boldsymbol{x})\\ -\left[Q_1^{N-n+1}(\boldsymbol{x},\boldsymbol{\xi}) + Q_2^{N-n}(\boldsymbol{x},\boldsymbol{\xi})\right]u^n(\boldsymbol{x})\end{pmatrix}\mathrm{d}\Gamma(\boldsymbol{x}) + u^{ff.N}(\boldsymbol{\xi}), \tag{6}$$

where $u^n(\boldsymbol{x})$ and $q^n(\boldsymbol{x})$ are displacement and traction fields on the boundary, respectively, $u^{ff.N}$ stands for the free field displacement at time $t = N\Delta t$, and $U_1^{N-n+1}(\boldsymbol{x},\boldsymbol{\xi}) + U_2^{N-n}(\boldsymbol{x},\boldsymbol{\xi})$ and $Q_1^{N-n+1}(\boldsymbol{x},\boldsymbol{\xi}) + Q_2^{N-n}(\boldsymbol{x},\boldsymbol{\xi})$ denote the half-plane displacement and traction time-convoluted kernels, respectively, as follows:

$$U_1^{N-n+1} + U_2^{N-n} = \frac{1}{2\pi}\left[\begin{pmatrix}(N-n+1)\cos h^{-1}\frac{(N-n+1)c\Delta t}{r} - \sqrt{(N-n+1)^2 - \left(\frac{r}{c\Delta t}\right)^2}\\ -2(N-n)\cos h^{-1}\frac{(N-n)c\Delta t}{r} + 2\sqrt{(N-n)^2 - \left(\frac{r}{c\Delta t}\right)^2}\\ +(N-n-1)\cos h^{-1}\frac{(N-n-1)c\Delta t}{r} - \sqrt{(N-n-1)^2 - \left(\frac{r}{c\Delta t}\right)^2}\end{pmatrix} + \begin{pmatrix}(N-n+1)\cos h^{-1}\frac{(N-n+1)c\Delta t}{r'} - \sqrt{(N-n+1)^2 - \left(\frac{r'}{c\Delta t}\right)^2}\\ -2(N-n)\cos h^{-1}\frac{(N-n)c\Delta t}{r'} + 2\sqrt{(N-n)^2 - \left(\frac{r'}{c\Delta t}\right)^2}\\ +(N-n-1)\cos h^{-1}\frac{(N-n-1)c\Delta t}{r'} - \sqrt{(N-n-1)^2 - \left(\frac{r'}{c\Delta t}\right)^2}\end{pmatrix}\right], \tag{7}$$

$$Q_1^{N-n+1} + Q_2^{N-n} = -\frac{1}{2\pi}\left[\begin{pmatrix}\frac{1}{r}\frac{\partial r}{\partial n}\left\{\begin{matrix}\sqrt{(N-n+1)^2 - \left(\frac{r}{c\Delta t}\right)^2} - 2\sqrt{(N-n)^2 - \left(\frac{r}{c\Delta t}\right)^2}\\ +\sqrt{(N-n-1)^2 - \left(\frac{r}{c\Delta t}\right)^2}\end{matrix}\right\}\end{pmatrix} + \begin{pmatrix}\frac{1}{r'}\frac{\partial r'}{\partial n}\left\{\begin{matrix}\sqrt{(N-n+1)^2 - \left(\frac{r'}{c\Delta t}\right)^2} - 2\sqrt{(N-n)^2 - \left(\frac{r'}{c\Delta t}\right)^2}\\ +\sqrt{(N-n-1)^2 - \left(\frac{r'}{c\Delta t}\right)^2}\end{matrix}\right\}\end{pmatrix}\right], \tag{8}$$

where r and r' are the distance from the source and the image source to the receiver point, respectively (Panji *et al.* 2013a), and n is the normal vector.

2.3.2 *Spatial integration*

All the calculations were conducted analytically until this part of the half-plane BEM formulation. To solve the spatial integral of eq. (6), boundary of the body was required to be discretized in a numerical scheme. After meshing the boundaries by M elements in utilizing the quadratic boundary elements, the above equation takes the following form:

$$c(\boldsymbol{\xi})\,u^N(\boldsymbol{\xi}) = \sum_{n=1}^{N}\sum_{m=1}^{M}\begin{bmatrix}\left\{\int_{\Gamma_m}\left[U_1^{N-n+1}[\boldsymbol{x}(\kappa),\boldsymbol{\xi}] + U_2^{N-n}[\boldsymbol{x}(\kappa),\boldsymbol{\xi}]\right]N_\alpha(\kappa)\,|J|\,\mathrm{d}\kappa\right\}q_\alpha^n\\ -\left\{\int_{\Gamma_m}\left[Q_1^{N-n+1}[\boldsymbol{x}(\kappa),\boldsymbol{\xi}] + Q_2^{N-n}[\boldsymbol{x}(\kappa),\boldsymbol{\xi}]\right]N_\alpha(\kappa)\,|J|\,\mathrm{d}\kappa\right\}u_\alpha^n\end{bmatrix} + u^{ff.N}(\boldsymbol{\xi}) \tag{9}$$

in which M represents total number of boundary elements, Γ_m stands for portion of the boundary to which element 'm' belongs, $N_\alpha(\kappa)$ is quadratic shape functions in terms of local intrinsic coordinates of κ ($\alpha = 1, 2, 3$) and J indicates Jacobian of transformation. Only in the first time step, when the collocation point (source) is in the integration element (receiver), numerical integration has a simple singularity issue (Panji *et al.* 2013a). In other cases, the integration can be carried out numerically using regular Gauss quadrature as well.

2.3.3 *Time stepping algorithm*

By taking spatial numerical integrals from eq. (9), the following matrix form can be obtained:

$$\sum_{n=1}^{N}\boldsymbol{H}^{N-n+1}\{\boldsymbol{u}^n\} = \sum_{n=1}^{N}\boldsymbol{G}^{N-n+1}\{\boldsymbol{q}^n\} + \left\{\boldsymbol{u}^{ff.N}\right\} \tag{10}$$

in which $\boldsymbol{H}^{N-n+1}$ and $\boldsymbol{G}^{N-n+1}$ are the matrices, the elements of which are determined by integration over the boundary elements, $\{\boldsymbol{u}^n\}$ and $\{\boldsymbol{q}^n\}$ are vectors of boundary nodal quantities in the time step n. $\left\{\boldsymbol{u}^{ff.N}\right\}$ is a matrix including free field displacements, which number of

columns is equal to number of time steps. In this form of eq. (10), the solution is not possible and the boundary conditions need to be applied in a numerical scheme for boundary nodes. After this procedure, eq. (10) takes the following soluble form:

$$\left[\boldsymbol{A}_1^1\right]\left\{\boldsymbol{X}^N\right\} = \left[\boldsymbol{B}_1^1\right]\left\{\boldsymbol{Y}^N\right\} + \left\{\boldsymbol{R}^N\right\} + \left\{\boldsymbol{u}^{ff.N}\right\}, \tag{11}$$

where $\left\{\boldsymbol{X}^N\right\}$ and $\left\{\boldsymbol{Y}^N\right\}$ are vectors of unknown and known boundary quantities, respectively, $\left[\boldsymbol{A}_1^1\right]$ and $\left[\boldsymbol{B}_1^1\right]$ are matrices, the columns of which correspond to unknown and known boundary quantities, respectively, and need to be only computed in the first time step. $\left\{\boldsymbol{R}^N\right\}$ denotes effects of past dynamic history on the current time node N, presented as follows:

$$\left\{\boldsymbol{R}^N\right\} = \sum_{n=1}^{N-1}\left(\boldsymbol{G}^{N-n+1}\left\{\boldsymbol{q}^n\right\} - \boldsymbol{H}^{N-n+1}\left\{\boldsymbol{u}^n\right\}\right). \tag{12}$$

By solving eq. (11) in each time step, all unknown boundary quantities including displacement and traction fields are obtained.

3 SUBSTRUCTURING PROCESS

The half-plane time-domain BEM approach shown in the above can be straightforwardly applied to obtain responses of topographies, the rough surfaces of which are placed below the ground surface. To solve topographies which boundaries are completely above the surface (convex topographies), a substructuring process was proposed. In this regard, as can be shown in Fig. 1, the convex topography must be divided into two parts. The first part is a half-plane including all surface/subsurface rough boundaries (such as concave topographies, embedded cavities, etc.) plus its interface with hill as an open domain model and the secondary part includes the mentioned interface together with elevated boundary as a closed domain model.

3.1 Domain I: an open media model

This domain must be modelled according to an open media scheme using half-plane time-domain BEM formulation and source image approach. Meshing direction must be appropriately applied to define the normal vector. As can be observed in Fig. 1, the model includes all rough surfaces or subsurfaces except the convex boundary. By considering that there are effects of incoming waves as well as outgoing ones, the discretized form of eq. (4) needs to be mentioned. After applying the half-plane BEM approach for Domain I, forming the considered matrices as eqs (10) and (11) and differentiating the nodes at all surface/subsurface rough boundaries (denoted by subscript 1) from those on the interface (denoted by subscript 12), the matrix form of this equation for time step $N = n$ can be obtained as:

$$\begin{bmatrix}\boldsymbol{H}_{12}^1 & \boldsymbol{H}_1^1\end{bmatrix}\begin{Bmatrix}\boldsymbol{u}_{12}^N\\ \boldsymbol{u}_1^N\end{Bmatrix} = \begin{bmatrix}\boldsymbol{G}_{12}^1 & \boldsymbol{G}_1^1\end{bmatrix}\begin{Bmatrix}\boldsymbol{q}_{12}^N\\ \boldsymbol{q}_1^N\end{Bmatrix} + \begin{Bmatrix}\boldsymbol{R}_{12}^N\\ \boldsymbol{R}_1^N\end{Bmatrix} + \begin{Bmatrix}\boldsymbol{u}_{12}^{ff.N}\\ \boldsymbol{u}_1^{ff.N}\end{Bmatrix} \tag{13}$$

so:

$$\left\{\boldsymbol{R}_{12}^N\right\} = \sum_{n=1}^{N-1}\left(\boldsymbol{G}_{12}^{N-n+1}\left\{\boldsymbol{q}_{12}^n\right\} - \boldsymbol{H}_{12}^{N-n+1}\left\{\boldsymbol{u}_{12}^n\right\}\right) \tag{14}$$

and

$$\left\{\boldsymbol{R}_1^N\right\} = \sum_{n=1}^{N-1}\left(\boldsymbol{G}_1^{N-n+1}\left\{\boldsymbol{q}_1^n\right\} - \boldsymbol{H}_1^{N-n+1}\left\{\boldsymbol{u}_1^n\right\}\right), \tag{15}$$

where $\boldsymbol{u}_{12}^N$ and $\boldsymbol{q}_{12}^N$ are displacements and tractions at the interface nodes for Domain I, respectively, $\boldsymbol{u}_1^N$ and $\boldsymbol{q}_1^N$ are displacements and tractions at all surface/subsurface rough boundaries, respectively. $\boldsymbol{R}_{12}^N$ and $\boldsymbol{R}_1^N$ denote past dynamic history on the current time node N and $\boldsymbol{u}_{12}^{ff.N}$ and $\boldsymbol{u}_1^{ff.N}$ indicate free field displacements for the interface nodes and all surface/subsurface rough boundaries, respectively.

3.2 Domain II: a closed media model

In the same way according to Domain I, this domain can be also modelled using half-plane time-domain BEM approach. But, there are some differences including the absence of free field motion in the equations (in the use of eq. 3 as BIE) and the direction of discretizing in order to close the domain. Thus, after conducting them, forming the matrices and also differentiating the nodes on the interface (denoted by subscript 21) from those on the convex boundary (denoted by subscript 2), the matrix form of BIE for time step $N = n$ can be written as:

$$\begin{bmatrix}\boldsymbol{H}_{21}^1 & \boldsymbol{H}_2^1\end{bmatrix}\begin{Bmatrix}\boldsymbol{u}_{21}^N\\ \boldsymbol{u}_2^N\end{Bmatrix} = \begin{bmatrix}\boldsymbol{G}_{21}^1 & \boldsymbol{G}_2^1\end{bmatrix}\begin{Bmatrix}\boldsymbol{q}_{21}^N\\ \boldsymbol{q}_2^N\end{Bmatrix} + \begin{Bmatrix}\boldsymbol{R}_{21}^N\\ \boldsymbol{R}_2^N\end{Bmatrix} \tag{16}$$

so:

$$\left\{\boldsymbol{R}_{21}^N\right\} = \sum_{n=1}^{N-1}\left(\boldsymbol{G}_{21}^{N-n+1}\left\{\boldsymbol{q}_{21}^n\right\} - \boldsymbol{H}_{21}^{N-n+1}\left\{\boldsymbol{u}_{21}^n\right\}\right) \tag{17}$$

and

$$\left\{\boldsymbol{R}_2^N\right\} = \sum_{n=1}^{N-1}\left(\boldsymbol{G}_2^{N-n+1}\left\{\boldsymbol{q}_2^n\right\} - \boldsymbol{H}_2^{N-n+1}\left\{\boldsymbol{u}_2^n\right\}\right), \tag{18}$$

where $\boldsymbol{u}_{21}^N$ and $\boldsymbol{q}_{21}^N$ are displacements and tractions at the interface nodes of Domain II, respectively, $\boldsymbol{u}_2^N$ and $\boldsymbol{q}_2^N$ are displacements and tractions on the convex boundary, respectively. $\boldsymbol{R}_{21}^N$ and $\boldsymbol{R}_2^N$ denote past dynamic history for the interface and hill surface nodes, respectively.

3.3 Assembling

To solve the problem and obtain the unknown fields, two series of above equations must be assembled in order to make an original coupled domain. For this purpose, it is required to satisfy continuity conditions at the interface. Compatibility and equilibrium conditions at the interface are as follows, respectively:

$$\boldsymbol{u}_{12}^N = \boldsymbol{u}_{21}^N \tag{19}$$

$$\mu_1 \boldsymbol{q}_{12}^N = -\mu_2 \boldsymbol{q}_{21}^N \tag{20}$$

where $\mu_1$and μ_2 are shear modules for Domains I and II, respectively. By considering that the problem needs to be homogeneously solved, it is assumed that μ_1 is equal to μ_2. After applying the continuity conditions at the interface, the matrix form of assembled BIEs can be written:

$$\begin{bmatrix} \boldsymbol{H}_{12}^1 & \boldsymbol{H}_1^1 & 0 & -\boldsymbol{G}_{12}^1 \\ \boldsymbol{H}_{21}^1 & 0 & \boldsymbol{H}_2^1 & \boldsymbol{G}_{21}^1 \end{bmatrix} \begin{Bmatrix} \boldsymbol{u}_{12}^N \\ \boldsymbol{u}_1^N \\ \boldsymbol{u}_2^N \\ \boldsymbol{q}_{12}^N \end{Bmatrix} = \begin{bmatrix} \boldsymbol{G}_1^1 & 0 \\ 0 & \boldsymbol{G}_2^1 \end{bmatrix} \begin{Bmatrix} \boldsymbol{q}_1^N \\ \boldsymbol{q}_2^N \end{Bmatrix} + \begin{Bmatrix} \boldsymbol{R}_{(1)}^N \\ \boldsymbol{R}_{(2)}^N \end{Bmatrix} + \begin{Bmatrix} \boldsymbol{u}_{(1)}^{ff.N} \\ 0 \end{Bmatrix} \tag{21}$$

in which:

$$\boldsymbol{R}_{(1)}^N = \begin{Bmatrix} \boldsymbol{R}_{12}^N \\ \boldsymbol{R}_1^N \end{Bmatrix} \tag{22}$$

$$\boldsymbol{R}_{(2)}^N = \begin{Bmatrix} \boldsymbol{R}_{21}^N \\ \boldsymbol{R}_2^N \end{Bmatrix} \tag{23}$$

$$\boldsymbol{u}_{(1)}^{ff.N} = \begin{Bmatrix} \boldsymbol{u}_{12}^{ff.N} \\ \boldsymbol{u}_1^{ff.N} \end{Bmatrix}, \tag{24}$$

where all variables considered in the above equations are the same as those observed in eqs (13) to (18). Boundary conditions on the convex surface as well as all surface/subsurface rough boundaries need to be satisfied in order to solve eq. (21). By considering that boundary conditions governing seismic problems are always of stress-free type ($\boldsymbol{q}_1^N = \boldsymbol{q}_2^N = 0$), eq. (21) can be rewritten in a simplified form as follows:

$$\begin{bmatrix} \boldsymbol{H}_{12}^1 & \boldsymbol{H}_1^1 & 0 & -\boldsymbol{G}_{12}^1 \\ \boldsymbol{H}_{21}^1 & 0 & \boldsymbol{H}_2^1 & \boldsymbol{G}_{21}^1 \end{bmatrix} \begin{Bmatrix} \boldsymbol{u}_{12}^N \\ \boldsymbol{u}_1^N \\ \boldsymbol{u}_2^N \\ \boldsymbol{q}_{12}^N \end{Bmatrix} = \begin{Bmatrix} \boldsymbol{R}_{(1)}^N \\ \boldsymbol{R}_{(2)}^N \end{Bmatrix} + \begin{Bmatrix} \boldsymbol{u}_{(1)}^{ff.N} \\ 0 \end{Bmatrix}. \tag{25}$$

After solving the above equations in each time step, all unknown quantities, such as displacements and tractions at the interface as well as displacements at all nodes belonging to convex and surface/subsurface rough boundaries, can be easily obtained. To find the responses at internal point m beyond the topography on the smooth ground surface, the discretized form of eq. (5) that is symbolized for Domain I can be written as:

$$\left\{\boldsymbol{u}^{N.m}\right\} = \sum_{n=1}^{N}\left(\begin{bmatrix} \boldsymbol{G}_{12}^{\langle N-n+1\rangle.m} & \boldsymbol{G}_1^{\langle N-n+1\rangle.m} \end{bmatrix} \begin{Bmatrix} \boldsymbol{q}_{12}^n \\ \boldsymbol{q}_1^n \end{Bmatrix}\right) - \sum_{n=1}^{N}\left(\begin{bmatrix} \boldsymbol{H}_{12}^{\langle N-n+1\rangle.m} & \boldsymbol{H}_1^{\langle N-n+1\rangle.m} \end{bmatrix} \begin{Bmatrix} \boldsymbol{u}_{12}^n \\ \boldsymbol{u}_1^n \end{Bmatrix}\right) + \begin{Bmatrix} \boldsymbol{u}_{12}^{ff.N.m} \\ \boldsymbol{u}_1^{ff.N.m} \end{Bmatrix}, \tag{26}$$

where $\boldsymbol{u}^{N.m}$ is displacement at internal point m. All parameters of eq. (26) correspond to eq. (13) so that only elements of their matrices depend on the location of internal points and boundary nodes. It is mentioned that, to obtain the responses at internal points, it is possible to use discretized form of eq. (16) for Domain II.

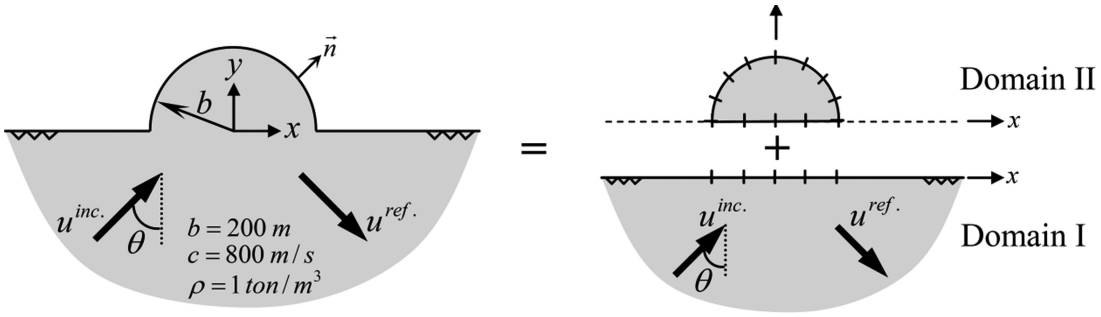

Figure 2. A definition sketch and schematic half-plane BEM model for a semi-circular cylindrical hill due to obliquely propagating incident *SH* waves.

4 VALIDATION EXAMPLES

The above-proposed half-plane time-domain BEM approach was implemented in a developed BE code called DASBEM and applied to investigate behaviour of convex topographies. Previously, capability and efficiency of this method were successfully verified for analysing concave surface topographies as well as embedded cavities (Panji *et al.* 2013a). In this section, its potentiality is presented for evaluating convex topographies. Three different known examples are solved and their results are compared with those of the published works.

4.1 A semi-circular cylindrical hill

In the first example, a semi-circular cylindrical hill subjected to obliquely propagating incident *SH* waves was considered, as in Fig. 2. The excitation wave's type was assumed according to Ricker wavelets function (Ricker 1953; Takemiya & Fujiwara 1994) as follows:

$$f(t) = \left[1 - 2\left(\pi f_p (t - t_0)\right)^2\right] \mathrm{e}^{-\left(\pi f_p (t-t_0)\right)^2} \tag{27}$$

in which f_p and t_0 are predominant frequency and time-shift parameter, respectively. According to the above function, the oblique antiplane displacements of incident *SH* waves are as:

$$u^{inc.}(x, y, t) = a_{\max} \cdot f\left(\alpha^{inc.}\right) H\left(t - \frac{r^{inc.}}{c}\right), \tag{28}$$

where $a_{\max}$ and $H(.)$ denote the maximum displacement time history and Heaviside function, respectively, and argument $\alpha^{inc.}$ is phase of incident waves in location $r^{inc.}$ and time t. c is also shear wave velocity. For satisfying the following stress-free conditions on the ground surface:

$$\frac{\partial u(x, y, t)}{\partial n} = \frac{\partial u^{ff}(x, y, t)}{\partial n} + \frac{\partial u^{sc}(x, y, t)}{\partial n} = 0, \tag{29}$$

where u^{ff} is free field displacement of ground surface and $u^{sc.}$ is contribution of scattered waves (can be computed by the proposed method); it is necessary to consider a reflected waves field with the reverse phase as follows:

$$u^{\mathrm{ref.}}(x, y, t) = a_{\max} \cdot f\left(\alpha^{\mathrm{ref.}}\right) H\left(t - \frac{r^{\mathrm{ref.}}}{c}\right), \tag{30}$$

where $u^{\mathrm{ref.}}(x, y, t)$ is the reflex displacement and $\alpha^{\mathrm{ref.}}$ denotes the phase of reflected waves in location $r^{\mathrm{ref.}}$ and time t. To obtain free field displacements denoted in eq. (4), the following can be written after adding eqs (28) and (30):

$$u^{ff}(x, y, t) = a_{\max} \cdot \left(\begin{array}{l} \left[1 - 2\left(\frac{\pi f_p}{c}\alpha^{\mathrm{inc.}}\right)^2\right] \mathrm{e}^{-\left(\frac{\pi f_p}{c}\alpha^{\mathrm{inc.}}\right)^2} H\left(t - \frac{r^{\mathrm{inc.}}}{c}\right) \\ + \left[1 - 2\left(\frac{\pi f_p}{c}\alpha^{\mathrm{ref.}}\right)^2\right] \mathrm{e}^{-\left(\frac{\pi f_p}{c}\alpha^{\mathrm{ref.}}\right)^2} H\left(t - \frac{r^{\mathrm{ref.}}}{c}\right) \end{array} \right) \tag{31}$$

in which:

$$\alpha^{\mathrm{inc.}} = c(t - t_0) + r^{\mathrm{inc.}}; \quad r^{\mathrm{inc.}} = -\sin\theta . x + \cos\theta . y, \tag{32}$$

and

$$\alpha^{\mathrm{ref.}} = c(t - t_0) + r^{\mathrm{ref.}}; \quad r^{\mathrm{ref.}} = -\sin\theta . x - \cos\theta . y, \tag{33}$$

where $u^{ff}(x, y, t)$ is free field displacement at coordinate (x, y) and time t. θ indicates the angle of incident waves, as in Fig. 2. To see stability of the proposed method versus changing the time step, coefficient β is measured as follows (Dominguez 1993):

$$\beta = \frac{c\Delta t}{\Delta l}, \tag{34}$$

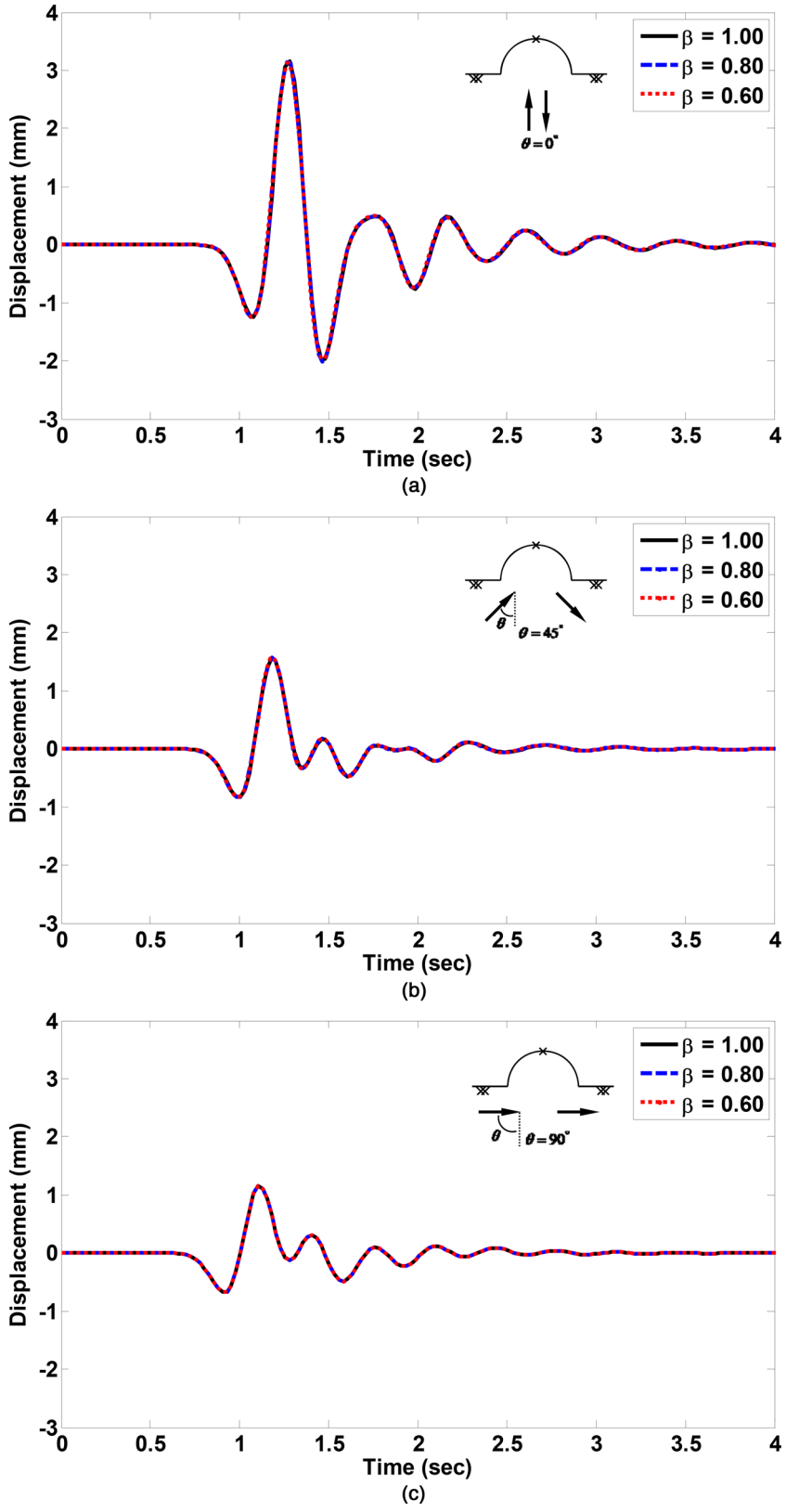

Figure 3. Transient response of the crest of semi-circular cylindrical hill subjected to oblique *SH* waves with three incidence angles: (a) 0°; (b) 45° and (c) 90°.

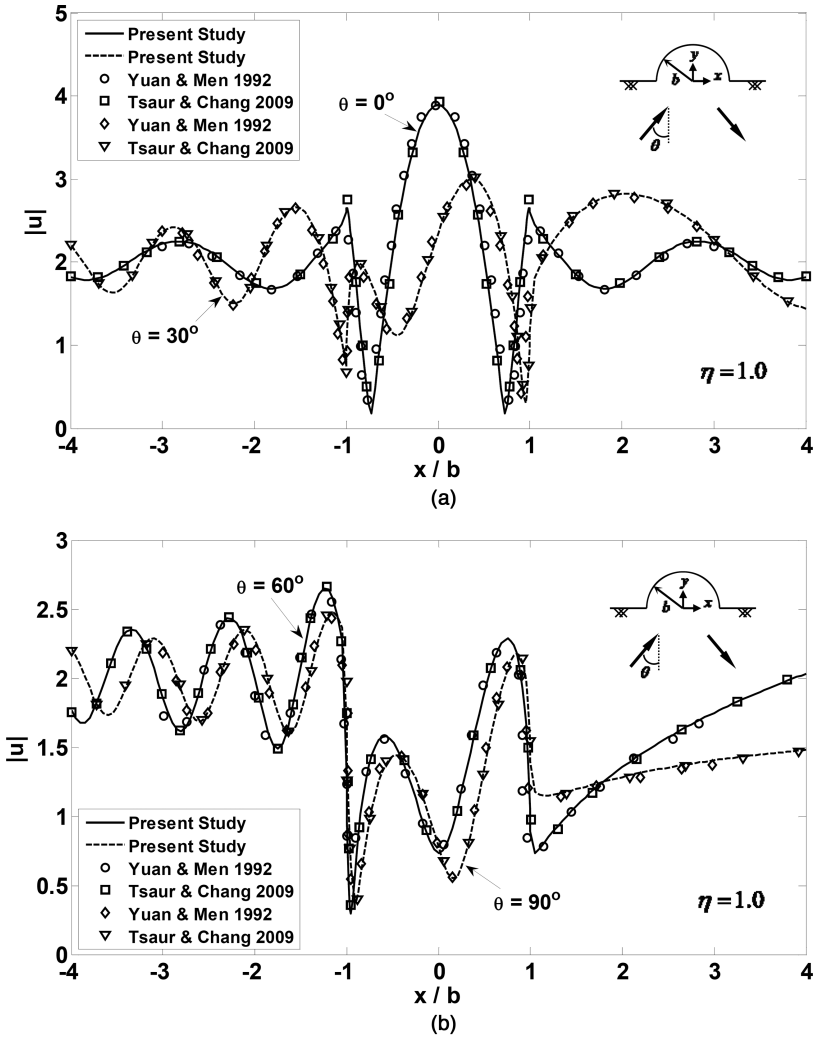

Figure 4. Normalized displacement amplitudes on the surface of semi-circular cylindrical hill at dimensionless frequency of 1.0 for the incidence angles: (a) 0° and 30°; (b) 60° and 90°.

where c, Δt and Δl are shear wave velocity, time step and distance of nodes, respectively. For time stepping analysis of elastodynamic problems with uniform meshing, it is recommended for this factor to be considered close to 1.0 (Dominguez & Gallego 1991). In this regard, by assuming shear wave velocity and nodes' distance of equal to 800 m s^{-1} and 20 m, respectively, the response convergence was investigated in three different time steps (0.025, 0.020 and 0.015 s). Hereby, the coefficient β had quantities of 1.0, 0.8 and 0.6, respectively. The predominant frequency, time-shift parameter and maximum amplitude of Ricker wavelet were equal to 3 Hz, 1.0 s, and 0.001 m, respectively. The results can be observed in Fig. 3. In this figure, the transient antiplane response of semi-circular hill apex is shown due to obliquely propagating incident *SH* waves including angels of 0°, 45° and 90°. As can be seen, stability of the method was favourable in different time steps. Therefore, to minimize the run time, time step was considered equal to 0.025 s in this example and the two next ones.

As can be observed in Fig. 2, the semi-circular hill was divided into two parts; a half-plane with the interface and a hill as the closed model. Taking nodes' interval of 20 m into account, the interface and exterior surface of the hill were discretized by 19 and 31 nodes, respectively. Twenty internal points were assigned to each side of the hill on the ground surface. The Ricker wavelet characteristics as well as time step were assumed according to the material of the previous paragraph. As shown in Fig. 2, in the use of half-plane time-domain BEM approach for the convex topography, the interface and hill surface are only necessary to be discretized.

To compare the results with those of the published works in the transformed domains, the dimensionless frequency needs to be defined as follows:

$$\eta = \frac{\omega b}{\pi c} \tag{35}$$

in which η is dimensionless frequency, ω is angular frequency of incident wave, b is half-width of the hill and c is shear wave velocity. In addition, normalized displacement amplitude is mostly used by researchers to present their results and it can be defined as ratio of the Fourier amplitude of the total motion to the Fourier amplitude of the input motion (denoted by $|u|$). For semi-circular cylindrical hill problem, Sills (1978) presented a numerical response using indirect frequency-domain full-plane BEM approach and Yuan & Men (1992) and Tsaur & Chang (2009) obtained analytical solutions in terms of wave function expansion. In Fig. 4, normalized displacements' amplitude of the

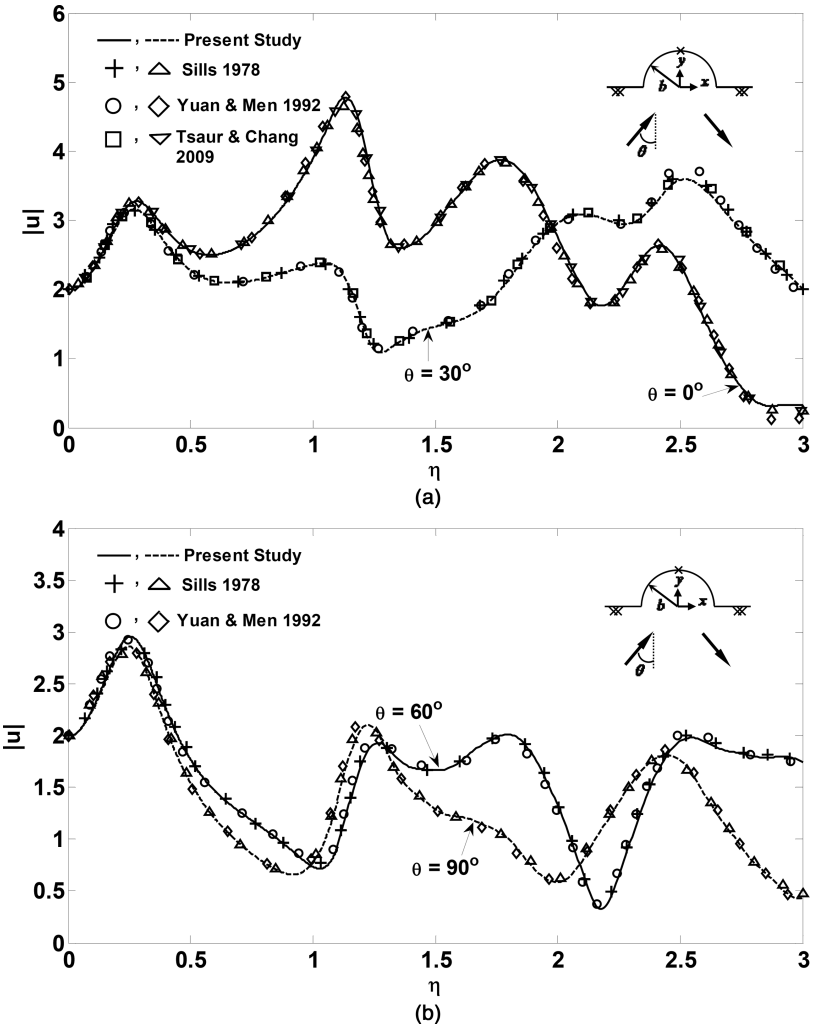

Figure 5. Normalized displacement amplitudes of the crest of semi-circular cylindrical hill versus η for the incidence angles: (a) 0° and 30°; (b) 60° and 90°.

ground surface in the range of $-4b \leq x \leq 4b$ is shown due to oblique incident *SH* waves including 0°, 30°, 60° and 90° at dimensionless frequency of 1.0 and compared with the mentioned solutions. As can be seen, the agreement with others was excellent and accuracy of the results was acceptable.

To demonstrate precision of the responses at different frequencies, Fig. 5 is presented. In this figure, displacements of the hill apex are presented versus dimensionless frequencies from 0.0 to 3.0. As can be observed, accuracy was favourable at all wave's angles. Capability of the proposed method at high frequencies can be also observed in Fig. 6. This figure displays normalized displacement amplitude of ground surface at dimensionless frequency of 5.0 for different wave angles and compares the present results with an analytical response. The results of Lee *et al.* (2006) were considered in this regard. They reported an improved analytic wave series solution for the semi-circular hill problem. As can be seen, the agreement was very good in a wide area of the surface.

One of the important topics in the BE analysis is the relation between node's distance and incident frequency. According to the assumed values for this example and the next ones, four segments per SH wavelength was proposed to analyse the problems by the half-plane time-domain BEM. In the other words, an acceptable response can be demonstrated in the dimensionless frequency of 5.0 (or actual frequency 10 Hz) by selecting nodes intervals less than $\lambda/4$ (λ is wavelength given by c/f, with c as shear wave velocity and f as actual frequency). For analysing a semi-circular valley using indirect full-plane BEM, Sanchez-Sesma & Campillo (1991) have suggested 15 segments per SV wavelength to obtain the stable solution at dimensionless frequency of 2.0, which it is remarkable compared to the present results. To determine the responses at higher dimensionless frequencies, for example at dimensionless frequency of 10, it is possible by reducing node's distance to 10 m.

4.2 A Gaussian-shaped ridge

Applicability of a numerical solution can be considerably appreciated when other methods are not able for their modelling. A Gaussian-shaped ridge with the following function perhaps can be only solved numerically:

$$y = h\left[1 - \left(\frac{x}{b}\right)^2\right] e^{-3\left(\frac{x}{b}\right)^2}, \tag{36}$$

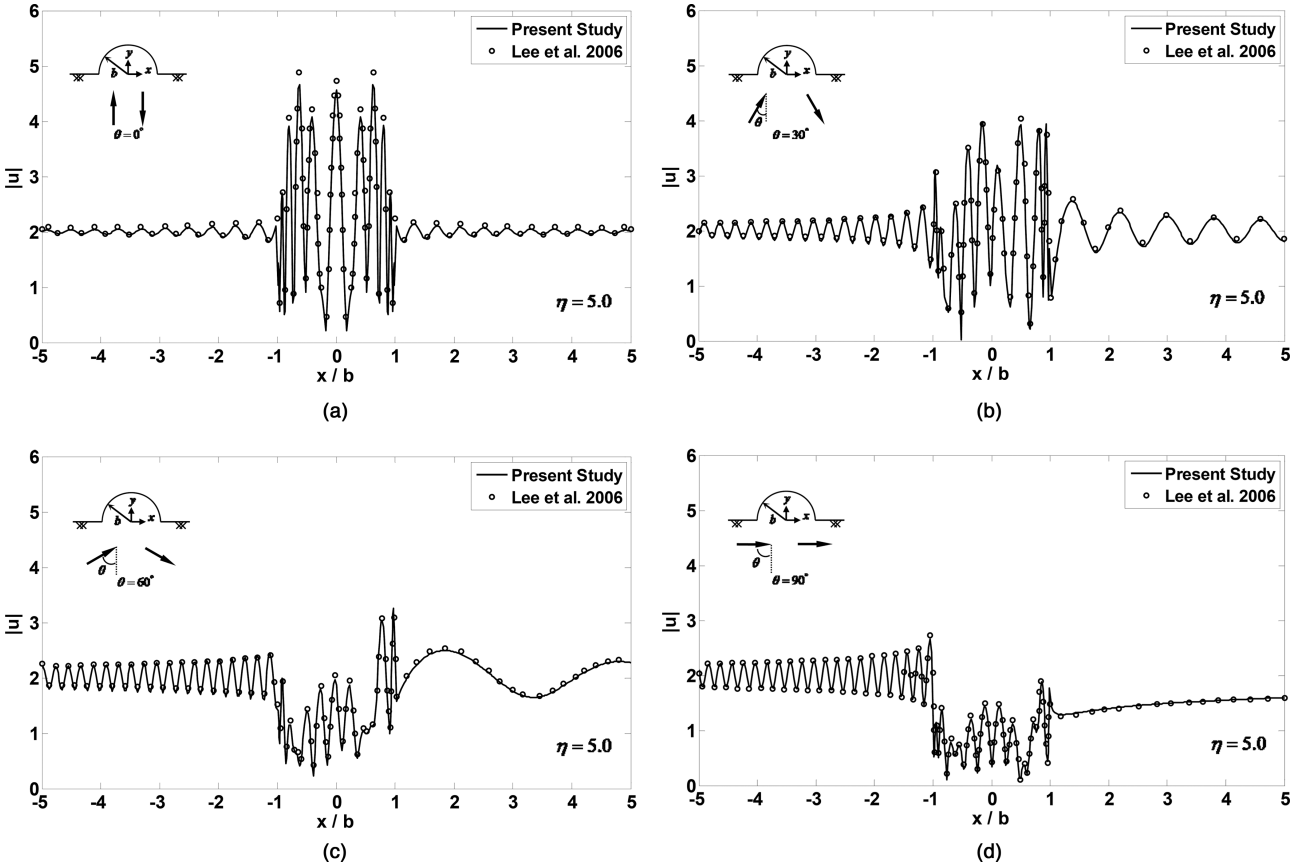

Figure 6. Normalized displacement amplitudes on the surface of semi-circular cylindrical hill at $\eta = 5.0$ compared with the results of Lee *et al.* (2006) for the incidence angles: (a) 0°; (b) 30°; (c) 60°; (d) 90°.

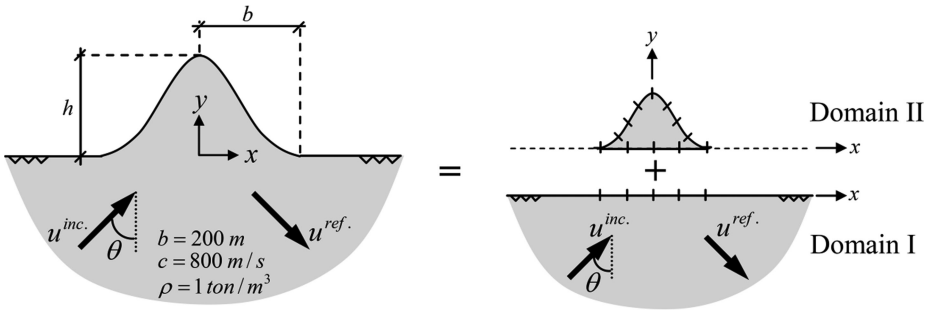

Figure 7. A definition sketch and schematic half-plane BEM model for a Gaussian-shaped ridge due to obliquely propagating incident SH waves.

where the curve is defined for $|x| \leq b$ and $y = 0$ in the case of $|x| > b$. h is height of the symmetrical ridge and b is half-width of the base. The model of the ridge is shown in Fig. 7. As can be observed, using half-plane BEM approach, only the ridge surface and its horizontal base need to be discretized. Here, according to what was considered by Sanchez-Sesma *et al.* (1982), three incident angles of 0°, 45° and 90° and three aspect ratios (h/b) equal to of 0.25, 0.50 and 0.75 were assumed. The interface was meshed by 19 nodes and the surface of the ridge was interrupted by 25, 21 and 15 nodes for the aspect ratios of 0.75, 0.50 and 0.25, respectively. The number of 20 internal points was considered on each side of the ridge on the smooth surface. Specifications of the Ricker wavelet were assumed similar to the previous example.

Fig. 8 shows normalized displacement amplitude on the surface of the ridges with different aspect ratios as well as various incident angles at dimensionless frequency of 0.5 and compares the results with numerical solution of Sanchez-Sesma *et al.* (1982). For solving Gaussian-shaped ridges, these researchers (Sanchez-Sesma *et al.* 1982) used an indirect boundary method in the frequency domain. Efficiency and capability of the presented method are completely detectable in Fig. 8, even for modelling these types of topography geometries.

4.3 A semi-circular hill joined by an inside concentric full/semi-circular cavity

As can be seen in two previous examples, half-plane BEM approach was able to model single convex topography. In this example, the potential of the method will be displayed for preparing those topography models that have multiple site effects. Therefore, a semi-circular cylindrical hill joined by an inside concentric full/semi-circular cavity was considered subjected to obliquely propagating incident *SH* waves

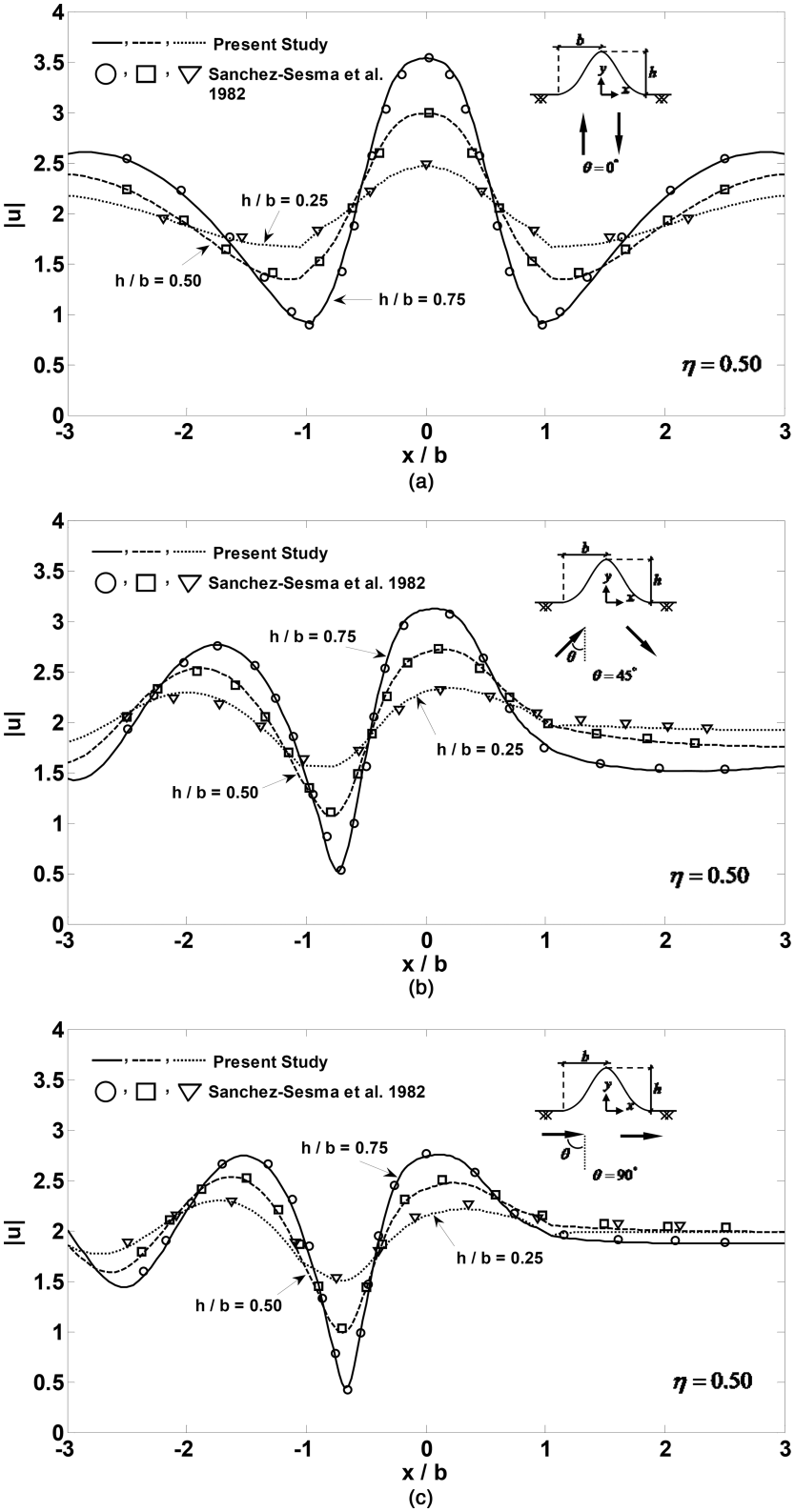

Figure 8. Normalized displacement amplitudes on the surface of Gaussian-shaped ridges with different aspect ratios at $\eta = 0.5$ compared with the results of Sanchez-Sesma *et al.* (1982) for the incidence angles: (a) 0°; (b) 45°; (c) 90°.

with different angles. Fig. 9 shows geometry of the models. First, the model of the hill with full-circular cavity was investigated and, next, semi-circular cavity case was discussed.

After separating the problem to two domains, the model was divided to a valley-shaped open medium and a half-cylinder-shaped closed medium (Fig. 9). By considering three different shape ratios (a/b) equal to of 0.20, 0.40 and 0.60, the models were elaborated totally by 57, 65 and 73 nodes, respectively. Accordingly, numbers of 16, 12 and 8 nodes were assigned to their interfaces, respectively, and the

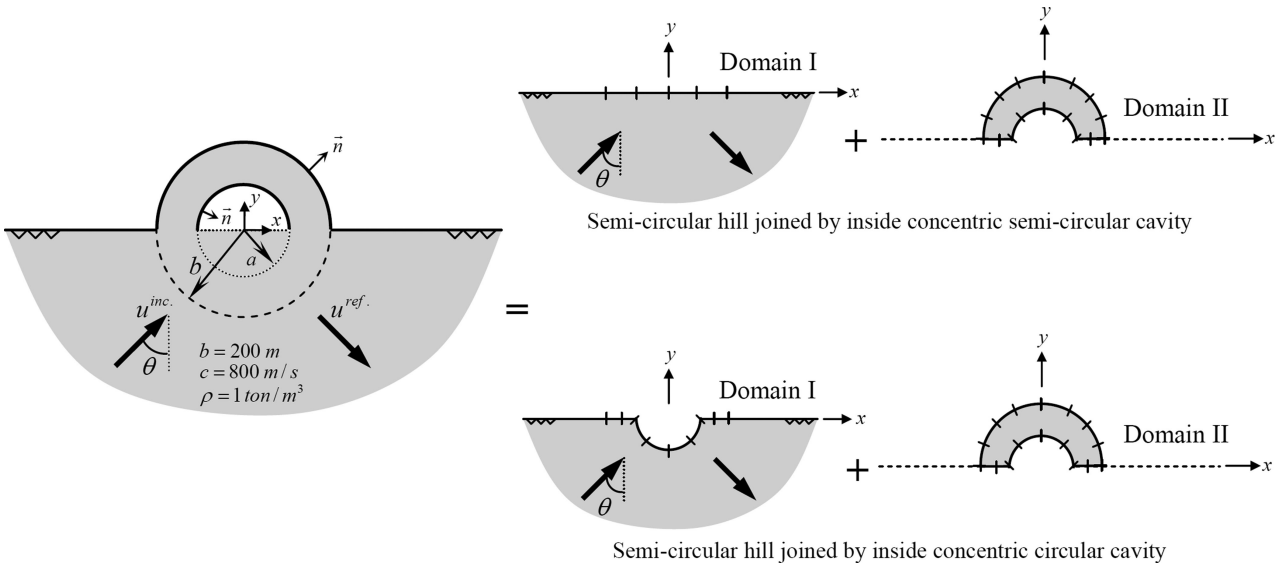

Figure 9. A definition sketch and schematic half-plane BEM model for a semi-circular cylindrical hill joined by an inside concentric full/semi-circular cavity due to obliquely propagating incident SH waves.

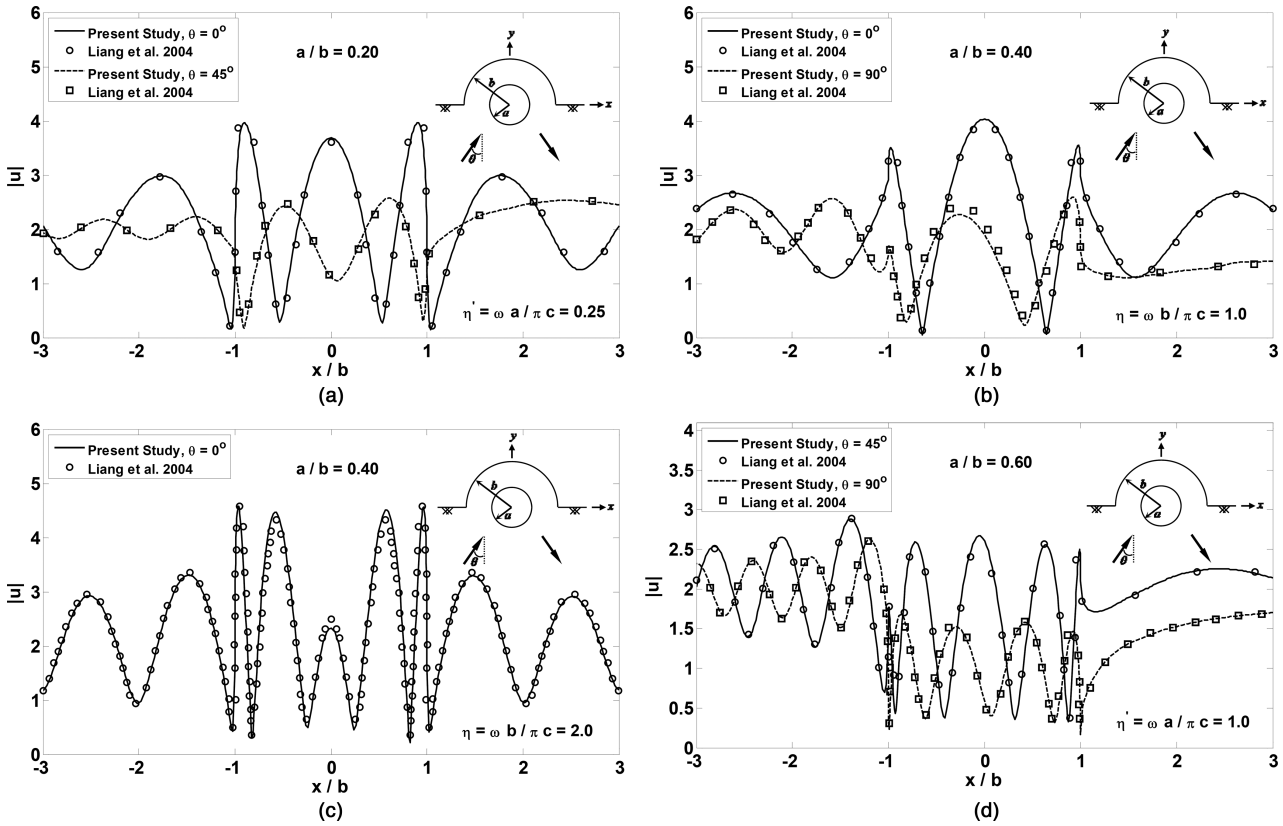

Figure 10. Normalized displacement amplitudes on the surface of a semi-circular cylindrical hill joined by an inside concentric circular cavity due to different incidence angels for comparison with the results of Liang *et al.* (2004) at: (a) $\eta' = 0.25$ and $a/b = 0.20$; (b) $\eta = 1.0$ and $a/b = 0.40$; (c) $\eta = 2.0$ and $a/b = 0.40$; (d) $\eta' = 1.0$ and $a/b = 0.60$.

remaining nodes were located on their cavities and hill surfaces. The Ricker parameters and material properties were as those considered for two previous examples. This problem was analytically solved by Liang *et al.* (2004). They presented a solution based on Fourier–Bessel series expansion and auxiliary functions technique. Fig. 10 shows normalized ground surface response in different shape ratios and dimensionless frequencies for the incident angles of 0°, 45° and 90°. As can be observed, the present results were in very good agreement with those of Liang *et al.* (2004). Only negligible disagreement was seen for angle 90° in $a/b = 0.40$ at top hill location. But, the errors were less than 7 per cent for the most critical state and it seems that they can be accepted.

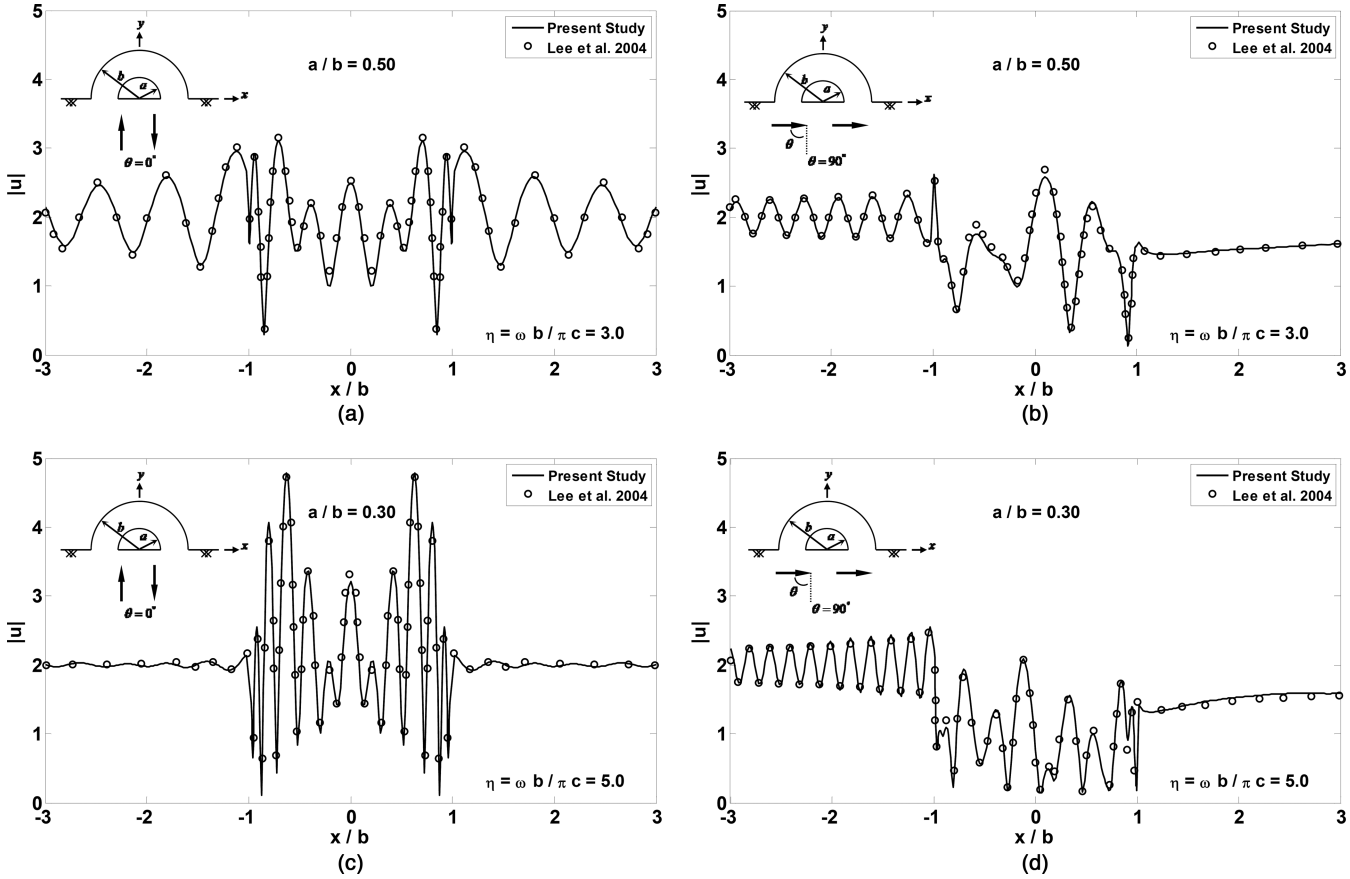

Figure 11. Normalized displacement amplitudes on the surface of a semi-circular cylindrical hill joined by an inside concentric semi-circular cavity for comparison with the results of Lee *et al.* (2004) at $\eta = 3.0$ and $\eta = 5.0$: (a) $a/b = 0.50$ and .; (b) $a/b = 0.50$ and $\theta = 90^\circ$; (c) $a/b = 0.30$ and $\theta = 0^\circ$; (d) $a/b = 0.30$ and $\theta = 90^\circ$.

For better compatibility of the analytical models with the nature, Lee *et al.* (2004) investigated a special case of full-circular cavity, that is, semi-circular cavity case one. They showed a closed-form analytic solution for semi-circular cylindrical hill with a concentric semi-circular cavity using the cylindrical wave functions' expansion method. The 2-D results by Lee *et al.* (2004) were presented in two shape ratios of $a/b = 0.30$, 0.50 and at two dimensionless frequencies of 3.0 and 5.0. To compare the present response with their results, Fig. 11 is demonstrated for some cases. This figure shows normalized displacement amplitude on the ground surface in the presence of a semi-circular hill joined by a semi-circular cavity with the mentioned shape ratios, due to incident *SH* waves including angles of 0° and 90°. As can be seen, accuracy of the results was very good compared with those by Lee *et al.* (2004). However, an insignificant error that can be again observed on the hill surface for shape ratio $a/b = 0.50$ at frequency of 3.0 is less than 7 per cent and it appears that the results can be certainly approved. It should be mentioned that the number of 55 and 63 nodes was totally used in modelling this geometry for shape ratios of 0.30 and 0.50, respectively, and the rest of the parameters were the same as previous examples.

4.4 Analysis time

Better capability and efficiency of the half-plane time-domain BEM approach as well as much shorter run time than traditional full-plane time-domain BEM have been investigated for analysing concave topographies (Panji *et al.* 2013a). In this section, a comparative study for analysis times of convex topographies models was conducted in completely the same conditions between the proposed method and a full-plane BEM approach (Table 1). In this regard, some of the models in the previous examples were prepared based on full-plane BEM approach (Kamalian *et al.* 2006; Kamalian *et al.* 2008a; Panji *et al.* 2013a) and their run times were evaluated. As can be seen in Table 1, in addition to decreasing total number of nodes to a quarter in modelling, the analysis time reduced considerably to one-fifth in the use of present method and it seems that run time difficulties in time-domain analysis can be promoted using half-plane time-domain BEM approach.

5 CONCLUSIONS

In this paper, a developed half-plane time-domain BEM was presented for analysing the 2-D convex topography features due to oblique incident *SH* waves. Using this method, only the interface and surface of the hill need to be discretized. First, using the proposed substructuring

Table 1. The CPU times in terms of second from executing time-domain (a) half-plane and (b) full-plane BEM code with an Intel Core i7 CPU M640 at 2.8 GHz and 4 GB RAM

(a)			NN[a]			
			Interface	Surfaces	Total	Time (s)
Example 1	A semi-circular cylindrical hill		19	31	50	115
		$h = 0.75b$	19	25	44	102
Example 2	A Gaussian-shaped ridge[b]	$h = 0.50$b	19	21	40	88
		$h = 0.25b$	19	15	34	72
	A semi-circular cylindrical hill	$a = 0.60b$	8	65	73	152
Example 3	joined by an inside concentric	$a = 0.40b$	12	53	65	138
	circular cavity[c]	$a = 0.20b$	16	41	57	129
(b)			NN			
			Surfaces	Ground surfaces	Total	Time (s)
Example 1	A semi-circular cylindrical hill		31	180	211	548
		$h = 0.75b$	25	180	205	523
Example 2	A Gaussian-shaped ridge	$h = 0.50b$	21	180	201	499
		$h = 0.25b$	15	180	195	480
	A semi-circular cylindrical hill	$a = 0.60b$	65	180	245	860
Example 3	joined by an inside concentric	$a = 0.40b$	53	180	233	725
	circular cavity	$a = 0.20b$	41	180	221	634

[a]NN indicates the number of nodes.
[b]Analysis times are presented in different aspect ratios (h/b) for the Gaussian-shaped ridge.
[c]Analysis times are presented in different shape ratios (a/b) for circular cavity.

process, the convex topography was divided into two domains, a half-space and a surface topography totally above the half-space. After applying the half-plane BEM approach for each domain and forming influence coefficients of the required matrices, the continuity conditions at the interface were satisfied in order to make an original coupled domain. Finally, by employing the boundary conditions at irregular surfaces, the problem was solved as well. Three interesting examples were examined to obtain capability and efficiency of the method. A semi-circular cylindrical hill, a Gaussian-shaped ridge and a semi-circular cylindrical hill joined by an inside concentric full/semi-circular cavity were investigated subjected to vertically as well as obliquely propagating incident *SH* waves as the Ricker wavelets type. By comparing the present results with those of the published works, it was seen that not only the method was successfully able to analyse these problems but also much shorter run time against full-plane BEM approach was determined. Due to absence of an interface in the topographies located completely below the ground surface, such as valley shaped features and embedded cavities, the half-plane BEM approach was straightforwardly able to model them in a simpler way compared to convex case (Panji *et al.* 2013a). But, the number of nodes that must be defined at the interface was very less than the number of nodes that was needed to be considered on the smooth surface in time-domain full-plane BEM approach (Kamalian *et al.* 2006, 2008a,b).

Although this paper was able to show application of the half-plane time-domain BEM approach for either convex or previously concave topographies, it is obvious that this method had also some important limitations in comparison with full-plane BEM approach. Due to the complexity of the half-space Green's function, they could not be simply extended to important cases such as anisotropic and viscoelastic media. This kind of problems could be solved more efficiently by the full-plane BEM.

As can be seen, the problems presented in this paper were solved with assumption of homogeneity; however, they could be non-homogenously investigated as well. The use of half-plane time-domain BEM for solving the non-homogeneous problems including alluvial valleys and multi-layered media with irregular interface can be interesting topics, which will be studied in future works.

ACKNOWLEDGEMENTS

The authors would like to express their gratitude to the respected editor, Prof Xiaofei Chen, and two anonymous reviewers for their useful comments and precious time spent on our paper.

REFERENCES

Ahmad, S. & Banerjee, P.K., 1988. Multi-domain BEM for two-dimensional problems of elastodynamics, *Int. J. Numer. Meth. Eng.,* **26**(4), 891–911.

Ausilio, E., Conte, E. & Dente, G., 2008. Seismic response of alluvial valleys to SH waves, in *Proceedings of the Seismic Engineering Conference, AIP Conference Proceedings,* Vol. 1020, pp. 199–206.

Bard, P.Y., 1982. Diffracted waves and displacement field over two-dimensional elevated topographies, *Geophys. J. R. astr. Soc.,* **71**(3), 731–760.

Belytschko, T. & Chang, H.S., 1988. Simplified direct time integration boundary element method, *J. Eng. Mech.,* **114**(1), 117–134.

Beskos, D.E., 1997. Boundary element methods in dynamic analysis: Part II (1986–1996), *Appl. Mech. Rev.,* **50**(3), 149–197.

Bouchon, M., 1973. Effect of topography on surface motion, *Bull. seism. Soc. Am.,* **63**(3), 615–632.

Brebbia, C.A. & Dominguez, J., 1989. *Boundary Elements, an Introductory Course,* Computational Mechanics Publications.

Chen, J.T., Lee, J.W. & Shyu, W.S., 2012. SH-wave scattering by a semi-elliptical hill using a null-field boundary integral equation method and a hybrid method, *Geophys. J. Int.,* **188**(1), 177–194.

Cole, D.M., Kosloff, D.D. & Minster, J.B., 1978. A numerical boundary integral method for elastodynamics, *Bull. seism. Soc. Am.,* **68**(5), 1331–1357.

Demirel, V. & Wang, S., 1987. An efficient boundary element method for two-dimensional transient wave propagation problems, *Appl. Math. Model.,* **11**(6), 411–416.

Dominguez, J., 1993. *Boundary Elements in Dynamics,* Computational Mechanics Publications.

Dominguez, J. & Gallego, R., 1991. The time domain boundary element method for elastodynamic problems, *Math. Comput. Model.,* **15**(3–5), 119–129.

Dominguez, J. & Meise, T., 1991. On the use of the BEM for wave propagation in infinite domains, *Eng. Anal. Bound. Elem.,* **8**(3), 132–138.

Dravinski, M., 1982. Influence of interface depth upon strong ground motion, *Bull. seism. Soc. Am.,* **72**(2), 597–614.

Eringen, A.C. & Suhubi, E.S., 1975. *Elastodynamics,* Academic Press.

Friedman, M.B. & Shaw, R., 1962. Diffraction of pulses by cylindrical obstacles of arbitrary cross section, *J. appl. Mech.,* **29** (1), 40–46.

Ge, Z.X. & Chen, X.F., 2007. Wave propagation in irregularly layered elastic models: a boundary element approach with a global refraction/transmission matrix propagator, *Bull. seism. Soc. Am.,* **97**(3), 1025–1031.

Ge, Z.X. & Chen, X.F., 2008. An efficient approach for simulating wave propagation with the boundary element method in multilayered media with irregular interfaces, *Bull. seism. Soc. Am.,* **98**(6), 3007–3016.

Geli, L., Bard, P.Y. & Jullien, B., 1988. The effect of topography on earthquake ground motion: a review and new results, *Bull. seism. Soc. Am.,* **78**(1), 42–63.

Hadley, P.K., Askar, A. & Cakmak, A.S., 1989. Scattering of waves by inclusions in a nonhomogeneous elastic half space solved by boundary element methods, Technical Report NCEER-89–0027.

Hirai, H., 1988. Analysis of transient response of SH wave scattering in a half-space by the boundary element method, *Eng. Anal.,* **5**(4), 189–194.

Israil, A.S.M. & Banerjee, P.K., 1990a. Advanced development of time-domain BEM for two-dimensional scalar wave propagation, *Int. J. Numer. Meth. Eng.,* **29**(5), 1003–1020.

Israil, A.S.M. & Banerjee, P.K., 1990b. Advanced time-domain formulation of BEM for two-dimensional transient elastodynamics, *Int. J. Numer. Meth. Eng.,* **29**(7), 1421–1440.

Jaramillo, J., Gomez, J., Saenz, M. & Vergara, J., 2013. Analytic approximation to the scattering of antiplane shear waves by free surfaces of arbitrary shape via superposition of incident, reflected and diffracted rays, *Geophys. J. Int.,* **192**(3), 1132–1143.

Kamalian, M., Gatmiri, B. & Sohrabi-Bidar, A., 2003. On time-domain two-dimensional site response analysis of topographic structures by BEM, *J. Seism. Earthq. Eng.,* **5**(2), 35–45.

Kamalian, M., Jafari, M.K., Sohrabi-Bidar, A., Razmkhah, A. & Gatmiri, B., 2006. Time-domain two-dimensional site response analysis of non-homogeneous topographic structures by a hybrid FE/BE method, *Soil Dyn. Earthq. Eng.,* **26**(8), 753–765.

Kamalian, M., Gatmiri, B., Sohrabi-Bidar, A. & Khalaj, A., 2007. Amplification pattern of 2D semi-sine shaped valleys subjected to vertically propagating incident waves, *Commun. Numer. Methods Eng.,* **23**(10), 871–887.

Kamalian, M., Jafari, M.K., Sohrabi-Bidar, A. & Razmkhah, A., 2008a. Seismic response of 2D semi-sines shaped hills to vertically propagating incident waves: amplification patterns and engineering applications, *Earthq. Spectra,* **24**(2), 405–430.

Kamalian, M., Sohrabi-Bidar, A., Razmkhah, A., Taghavi, A. & Rahmani, I., 2008b. Considerations on seismic microzonation in areas with two-dimensional hills, *J. Earth Syst. Sci.,* **117**(2), 783–796.

Kawase, H., 1988. Time-domain response of a semi-circular canyon for incident SV, P, and Rayleigh waves calculated by the discrete wavenumber boundary element method, *Bull. seism. Soc. Am.,* **78**(4), 1415–1437.

Lee, V.W., Luo, H. & Liang, J.W., 2004. Diffraction of antiplane SH waves by a semicircular cylindrical hill with an inside concentric semicircular tunnel, *Earthq. Eng. Eng. Vibr.,* **3**(2), 249–262.

Lee, V.W., Luo, H. & Liang, J.W., 2006. Antiplane (SH) waves diffraction by a semicircular cylindrical hill revisited: an improved analytic wave series solution, *J. Eng. Mech.,* **132**(10), 1106–1114.

Liang, J.W., Luo, H. & Lee, V.W., 2004. Scattering of SH waves by a circular-arc hill with a circular tunnel, *Acta Seismol. Sin.,* **17**(5), 549–563.

Liu, G., Chen, H., Liu, D. & Khoo, B.C., 2010. Surface motion of a half-space with triangular and semicircular hills under incident SH waves, *Bull. seism. Soc. Am.,* **100**(3), 1306–1319.

Mansur, W.J. & Brebbia, C.A., 1982a. Formulation of the boundary element method for transient problems governed by the scalar wave equation, *Appl. Math. Model.,* **6**(4), 307–311.

Mansur, W.J. & Brebbia, C.A., 1982b. Numerical implementation of the boundary element method for two-dimensional transient scalar wave propagation problems, *Appl. Math. Model.,* **6**(4), 299–306.

Mogi, H. & Kawakami, H., 2007. Analysis of scattered waves on ground with irregular topography using direct boundary element method and Neumann series expansion, *Bull. seism. Soc. Am.,* **97**(4), 1144–1157.

Morse, P.M. & Feshbach, H., 1953. *Methods of Theoretical Physics,* McGraw-Hill Book Company.

Ohtsu, M. & Uesugi, S., 1985. Analysis of SH wave scattering in a half space and its applications to seismic responses of geological structures, *Eng. Anal.,* **2**(4), 198–204.

Panji, M., Kamalian, M., Asgari Marnani, J. & Jafari, M.K., 2013a. Transient analysis of wave propagation problems by half-plane BEM, *Geophys. J. Int.,* **194**(3), 1849–1865.

Panji, M., Kamalian, M., Asgari Marnani, J. & Jafari, M.K., 2013b. Antiplane seismic response from semi-sine shaped valley above embedded truncated circular cavity: a time-domain half-plane BEM, *Int. J. Civil Eng.,* in review.

Panji, M., Kamalian, M., Asgari Marnani, J. & Jafari, M.K., 2013c. Amplification pattern of semi-sine shaped valleys to vertically propagating incident *SH* waves, *J. Comput. Methods Eng.,* **32**(2), 1–25 (in Persian).

Reinoso, E., Wrobel, L.C. & Power, H., 1993. Preliminary results of the modeling of the Mexico City valley with a two-dimensional boundary element method for the scattering of SH Waves, *Soil Dyn. Earthq. Eng.,* **12**(8), 457–468.

Ricker, N., 1953. The form and laws of propagation of seismic wavelets, *Geophysics,* **18**(1), 10–40.

Sabina, F.J. & Willis, J.R., 1975. Scattering of SH waves by a rough half-space of arbitrary slope, *Geophys. J. R. astr. Soc.,* **42**(2), 685–703.

Sanchez-Sesma, F.J. & Campillo, M., 1991. Diffraction of P, SV, and Rayleigh waves by topographic features: a boundary integral formulation, *Bull. seism. Soc. Am.,* **81**(6), 2234–2253.

Sanchez-Sesma, F.J. & Esquivel, J.A., 1979. Ground motion on alluvial valleys under incident plane SH waves, *Bull. seism. Soc. Am.,* **69**(4), 1107–1120.

Sanchez-Sesma, F.J., Herrera, I. & Aviles, J., 1982. A boundary method for elastic wave diffraction: application to scattering of SH waves by surface irregularities, *Bull. seism. Soc. Am.,* **72**(2), 473–490.

Sanchez-Sesma, F.J., Palencia, V.J. & Luzon, F., 2002. Estimation of local site effects during earthquakes: an overview, *ISET J. Earthq. Technol.,* **39**(3), 167–193.

Sills, L.B., 1978. Scattering of horizontally-polarized shear waves by surface irregularities, *Geophys. J. R. astr. Soc.,* **54**(2), 319–348.

Soares, D. Jr. & Mansur, W.J., 2009. An efficient time-truncated boundary element formulation applied to the solution of the two-dimensional scalar wave equation, *Eng. Anal. Bound. Elem.,* **33**(1), 43–53.

Takemiya, H. & Fujiwara, A., 1994. SH-Wave scattering and propagation analysis at irregular sites by time domain BEM, *Bull. seism. Soc. Am.,* **84**(5), 1443–1455.

Tsaur, D.H. & Chang, K.H., 2009. Scattering and focusing of SH waves by a convex circular-arc topography, *Geophys. J. Int.,* **177**(1), 222–234.

Wong, H.L. & Jennings, P.C., 1975. Effects of canyon topography on strong ground motion, *Bull. seism. Soc. Am.,* **65**(5), 1239–1257.

Yu, G., Mansur, W.J., Carrer, J.A.M. & Gong, L., 2000. Stability of Galerkin and collocation time domain boundary element methods as applied to the scalar wave equation, *Comput. Struct.,* **74**(4), 495–506.

Yuan, X. & Liao, Z.P., 1996. Surface motion of a cylindrical hill of circular-arc cross-section for incident plane SH waves, *Soil Dyn. Earthq. Eng.,* **15**(3), 189–199.

Yuan, X. & Men, F.L., 1992. Scattering of plane SH waves by a semi-cylindrical hill, *Earthq. Eng. Struct. Dyn.,* **21**(12), 1091–1098.

Zhou, H. & Chen, X.F., 2006. A new approach to simulate scattering of SH waves by an irregular topography, *Geophys. J. Int.,* **164**(2), 449–459.

Zhou, H. & Chen, X.F., 2008. The localized boundary integral equation-discrete wavenumber method for simulating P-SV wave scattering by an irregular topography, *Bull. seism. Soc. Am.,* **98**(1), 265–279.